AADE-18-FTCE-117

In-Situ Property Enhancement of Smart Spacer Fluid Modified with Iron Oxide Nanoparticles for Cleaning Bentonite Contamination and Characterized Using the Vipulanandan Rheological Model

C. Vipulanandan and A.R. Maddi, Center for Innovative Grouting Materials and Technology (CIGMAT) and Texas Hurricane Center for Innovative Technology (THC-IT) - University of Houston.

Abstract

Oil and gas Production wells are facing numerous problems to have a successful well cementing operation. The condition of the cementing is dependent on the well cleaning performed using the spacer fluids. Use of spacer fluids to improve the cementing job has gained importance in deep well drilling. The contamination of spacer fluids by the drilling muds reduces the efficiency of the cleaning job and hence is in need of real time monitoring. Based on the depth applications, different types of spacer fluids are available in the oil gas industry. In this experimental study modifying the smart spacer fluid properties in-situ was investigated. Optimization of spacer formulation was carried by having material properties such as density, rheology and cleaning efficiencies as the variables. In this study, new monitoring parameter electrical resistivity was investigated to quantify the cleaning efficiencies of spacer formulations and drilling fluids.

In this study, smart spacer fluid was modified with iron oxide nanoparticles (nanoFe_2O_3) to enhance the performance under varying pressure, temperature and magnetic field strengths. Also the cleaning of bentonite contamination from the drilling mud using the modified smart spacer fluids were investigated. The temperature was varied from 25°C to 75°C. The magnetic field strength was varied from 0 T to 0.6 T. The amount of bentonite contamination was varied from 0 to 0.5% by weight of the spacer. The nanoFe_2O_3 contents (particle size of 30 nm and surface area of 38 m^2/gm) in the spacer fluid were varied up to 1% by the weight of spacer fluid to enhance the sensing and rheological properties of the spacer fluid. The initial resistivity of the spacer fluid without any nanoFe2O3 at 25°C was 0.2 Ω-m. Addition of 1% nanoFe_2O_3 increased the electrical resistivity by 3.5%. Adding nanoFe_2O_3 enhanced the piezoresistive behavior of the smart spacer fluid. The electrical resistivity changed by 0.7 and 12% for the spacer fluids with 0 and 1% nanoFe_2O_3 for a maximum pressure of 500 psi.

Increase in the magnetic field strength improved the rheological properties while increasing the temperature decreased the rheological properties of the spacer. The spacer fluid with nanoFe_2O_3 exhibited better rheological properties compared to the spacer fluid without nano iron oxide particles. The rheological properties of the spacer fluids were characterized by high strain rate to determine the nonlinear behavior of the shear thinning spacer fluid. The spacer fluid rheology was modelled using Bingham-plastic model, Hershel Bulkley model and Vipulanandan model. The electrical resistivity was used as sensing parameter to monitor the percentage of oil cleaning efficiency of the spacer fluid. Based on the new Vipulanandan rheological model, the yield stress (τ_o) of the modified spacer fluid increased by 14% to 98% depending on the bentonite contamination, nanoFe_2O_3 content, temperature and magnetic field strength. The τ_{max} for the spacer fluid increased from 49.4 Pa to 65.5 Pa, 33% increase at the temperature of 25°C with 1% addition of nanoFe_2O_3.The cleaning efficiency of the spacer fluid was 82.3% without the addition of nanoFe_2O_3. With the addition of nanoFe_2O_3 the cleaning efficiency increased from 82.3 to 98.5%, 16.2% increase in the efficiency. The maximum shear stress tolerance (τ_{max}) correlated well with the cleaning efficiency. Also the change in the electrical resistivity of the spacer fluid after cleaning correlated well with the cleaning efficiency and hence can be used for in-situ monitoring of the cleaning operation.

Introduction

For successful cementing the space between the steel casing and geological formation must be clean. Spacer fluids have been primarily developed to separate the cement slurry from the drilling fluid because of contamination of the cement affecting the cementing operation and long-term stability of the cemented wells. Incompatibility in the fluids can cause significant increase in the viscosity, and thus hydraulic resistance inside the wellbore. Efficient displacement and effective removal of the drilling fluids and associated residues from the wellbore prior to the completion of a well is critical for optimized hydrocarbon recovery (Quintero, Christian et al, 2008). There are several benefits in using drilling mud in drilling operations but there are concerns about potential contamination of the spacer and cement (Vipulanandan and Amani, 2015). Also, cements are sensitive to drilling fluid contaminations and therefore even a thin layer of drilling fluid

could prevent the cement from bonding to the formation and the casing. Effective displacement of the synthetic or oil based drilling mud is extremely important in order to minimize non-productive time (NPT), reduce waste volume, to prevent cement failures and to reduce the risk of completion tool complications (Quintero et al, 2012).

The cleaning depends on the type of drilling fluids and the geological formation. Selecting the proper spacer fluid is typically important and is dependent on the chemistry of the drilling fluid, its composition and conditions of the well. Spacer fluids play a crucial role in proper cementing job by complete displacement of the drilling mud and removal of the filter cake developed along the formation. Various types of spacer systems are available in the oil and gas industry, but they may not be suitable for changing conditions with depth. The spacer design can be changed according to different conditions including geological condition of the well; however it should be designed for a specific density, mud system, cement system and rheology. Generally a spacer fluid is composed of the following components. (1)Water/Oil as the base fluid of spacer system; (2) Weighting materials to increase the density of the spacer system; (3) Rheological modification agent or polymers and (4) A proper surfactant Package. Using these components in the spacer fluid makes the spacer density and rheological properties fall in between the density and rheological profile of drilling fluid and cement (Zanten et al, 2011)

During recent years the operators are to explore and produce from increasingly more difficult environments. Fluid displacements in offshore environments require spacer fluids to perform more than one operation effectively at low and high temperatures encountered in the well. In each of these cases there have to be a novel design to adjust for different conditions. Use of nanoparticles in spacer system can provide enhancements in rheological, thermal, mechanical, magnetic and optical profiles. Nanoparticles with noticeable alterations in the optical, magnetic field strength and electrical properties are excellent tools for the development of sensors and the formation of imaging contrast. Since the nanoparticles are extremely small in size, nanoparticles are preferred to be used in the oil and gas industry as their abrasive forces are negligible with less kinetic energy impact. The nanoparticles are added to the mud in small amount, with the concentration of the order of 1%. Nano-based drilling muds could be the fluid of choice in conducting drilling operations in sensitive environments to protect other natural resources. Recent studies have shown that when nanomaterials are added to the drilling muds it can be used as a sensing material downhole for temperature and pressure (Vipulanandan and Mohammed, 2017). Nanotechnology is increasingly being deployed in hydraulic fracturing of conventional and unconventional wells. Most of the proposed applications of nanotechnology in the oil field can be classified into the following areas of sensing or imaging, enhanced oil recovery, gas mobility control, drilling, and completion and produced fluid treatment.

Mathematical modeling studies have been related to the well and pipeline flow of thixotropic drilling muds, spacer fluids and crude oils. Spacer fluids exhibit complex rheological behavior and have been modelled using the Bingham model (1919) or Herschel-Bulkley model (1926). The limitations of the mathematical modeling studies concerning thixotropic drilling mud and crude oil flows have two main causes. Despite recent advancements in tools such as quality HTHP/LT (high-temperature/high-pressure/low-temperature) viscometers, a unified rheological model valid for a wide range of pressures, temperatures, and flow regimes which could account for complex rheological effects such as thixotropic and shear stress limits still does not exist (Livescu 2012). Spacer fluid properties such as shear stress and shear strain rate relationship, yield stress and maximum shear stress concerning thixotropic spacer fluid and crude oil flows have two main causes. Spacer fluid properties such as shear stress and shear strain rate relationship, yield stress and maximum shear stress play an important role in designing and optimizing the performance of spacer fluids. Non-Newtonian fluids do not conform to direct proportionality between shear stress and shear strain rate and there are limitations on the relationships that are being used to describe the rheological properties of spacer fluids. Recently a new Vipulanandan rheological model (2014) has been developed for shear thinning fluids where the shear stress-shear strain rate relationship is nonlinear with a limit on the maximum shear stress tolerance (Vipulanandan and Mohammed, 2014a).

Objective

To develop and characterize highly sensing smart spacer fluids with nanoFe_2O_3 for in – situ sensing and property modifications.

The specific objectives are as follows:

(i) Design spacer fluid with higher cleaning efficiency (>95%) for bentonite drilling fluid using iron nanoparticles.

(ii) Investigate the effects of magnetic field and temperature on the sensing and rheology property modifications.

(iii) Investigate the relationship between cleaning efficiency and spacer fluid property and also correlation between the electrical resistivity of the spacer fluid contamination so that it can be used as a real-time monitoring parameter.

Materials and Methods

Spacer Fluid Preparation

The spacer fluid was prepared by using water as the base fluid. Rheology modifiers such as Guargum upto 1% and UH bio-surfactant upto 0.4% were added. Also upto 3% KCL

was added with the weighting agent lead nitrate ($Pb(NO_3)_2$). KCl was first mixed with water till it completely dissolves. Then rheology modifier Guargum was added followed with the UH Bio-surfactant and mixed until uniform solution is obtained. This uniform mixture is then mixed with the weighting agent to obtain the spacer fluid. Also, nanoiron was added to the spacer fluid to enhance the performance with pressure, temperature and magnetic field. Also the fluid was characterized with electrical resistivity and density measurements at each stage of mixing.

UH Biosurfactant

The biosurfactant is produced from waste oil with acclimated bacteria in continuously stirred batch reactor (Harendra et al. 2008; Vipulanandan et al. 2000). The critical micelle concentration (CMC) for this biosurfactant is 0.5 g/L and the surface tension reduces to 30 dynes/cm. The biosurfactant is water soluble and based on Fourier Transform Infra Read (FTIR) spectroscopy analyses both carboxyl (COO-) and hydroxide (OH-) groups were identified in the biosurfactant.

Water Based Drilling Fluid

The water based drilling fluid is prepared by addition of 8% bentonite by weight of water. The density and resistivity of the drilling fluid was 8.2 ppg and 7 Ω-m.

Density

The density plays a major role in providing the needed hydrostatic pressure in the wellbore. Density of the spacer fluid with and without nanoiron was measured immediately after mixing using the standard mud balance cup.

Electrical Resistivity

Two different instruments were used to measure the electrical resistivity of the spacer fluid. The instruments were calibrated using standard salt solution**.**

(a)*Conductivity Probe*

A commercially available conductivity probe was used to measure the conductivity (inverse of electrical resistivity) of the fluids. The conductivity measuring range was from 0.1μS/cm to 1000 mS/cm, representing a resistivity of 1,000 Ω-m to 0.1 Ω-m, respectively**.**

(b)*Digital Resistivity Meter*

The digital resistivity meter measured the resistivity of fluids, slurries, and semi-solids with resistivities in the range of 0.01Ω-m to 400 Ω-m.

HPHT Testing

The spacer fluid was subjected to pressures of 500 psi. The change in the bulk resistivity of the material was measured and modelled using Vipulanandan model.

Rheological Properties

Rheological properties determine the pumpability and cleaning capability of spacer. The rheology tests for smart spacer fluid with different contents of nanoiron ($nanoFe_2O_3$) at temperature of 25°C to 75°C and magnetic fields of 0 to 0.6T were tested using a viscometer in the speed range of 0.3 to 600 rpm (shear strain rate of 0.5 s^{-1} to 1024 s^{-1}) and related shear stresses were recorded. The speed accuracy of this device was 0.001 rpm. The temperature of the spacer was controlled to an accuracy of ±2˚C. The viscometer was calibrated using several standard solutions. All the rheological tests were performed after 10 minutes of mixing of the spacer solutions. The viscometer was calibrated using several standard solutions.

Cleaning efficiency test

The cleaning efficiency test was performed on the spacer fluid to quantify the ability of the spacer to clean the bentonite drilling fluid. For this test the following procedure was followed.

Initially the viscometer cup and bob were made clean and dry. Then the empty weight of the bob (W1) was measured. The viscometer cup was filled with bentonite drilling fluid and run for 10 minutes at 100 rpm. After 10 minutes, the viscometer bob again (with the bentonite drilling fluid) (W2) was weighted again. Then the Spacer fluid was placed in the cup and the viscometer was rotated again for 10 minutes at 100 rpm. Then the viscometer bob was weighted again (W3). Also the changes in the resistivity of the cleaning spacer fluid were measured.

The cleaning efficiency of the spacer is calculated using the following formula.

$$\textbf{Cleaning efficiency}(\%) = \frac{\mathbf{W_2 - W_3}}{\mathbf{W_2 - W_1}} * \mathbf{100}$$

Modeling

Rheological Modeling

The spacer fluid showed non-linear shear thinning behavior with a yield stress. Based on the test results, following conditions have to be satisfied for the model to represent the observed behavior.

Hence the conditions are as follows:

$\tau = \tau_o$ when $\dot{\gamma} = 0$

$$\frac{d\tau}{d\dot{\gamma}} > 0, \quad (1)$$

$$\frac{d^2\tau}{d\dot{\gamma}^2} < 0 \text{ ,and} \quad (2)$$

$$\dot{\gamma} \to \infty \Rightarrow \tau = \tau^*. \quad (3)$$

The rheological models used for predicating the shear thinning behavior of foam cement slurry are as follows:

Herschel-Bulkley model (1926)

The Bingham plastic model includes both yield stress (τ_o) and a limiting viscosity (μ) at finite shear rates, which the Power law model fails to consider. For a nonlinear flow relationship shear-thinning or shear thickening behavior may be observed and the assumption of constant plastic viscosity is not valid. The Herschel-Bulkley (Eqn. 4) model defines a fluid with three parameters and can be represented mathematically as

$$\tau = \tau_{o1} + k * (\dot{\gamma})^n, \quad (4)$$

where τ , τ_{o1}, $\dot{\gamma}$, k and n represent the shear stress, yield stress, shear strain rate, correction parameter and flow behavior index respectively. For $\tau < \tau_o$ the material remains rigid. The model assumes that below the yield stress (τ_o), the slurry behaves as a rigid solid, similar to the Bingham plastic model. For $\tau > \tau_o$ the material flows as a Power law fluid. The exponent n describes the shear thinning and shear thickening behavior. Slurries are considered as shear thinning when n <1 and shear thickening when n >1. A fluid becomes shear thinning when the apparent viscosity decreases with the increase in shear strain rate.

Hence the model should satisfy the following conditions (Eqns. (1), (2) and (3)).

Applying the conditions, we have

$$\frac{d\tau}{d\dot{\gamma}} = k*n*\dot{\gamma}^{(n-1)} > 0 \Rightarrow k*n > 0 \text{ and} \quad (5)$$

$$\frac{d^2\tau}{d\dot{\gamma}^2} = k*n(n-1)*\dot{\gamma}^{(n-2)} \Rightarrow \mathrm{k*n*(n-1)} < 0. \quad (6)$$

One condition when both Eqn. (5) and Eqn. (6) will be satisfied is as follows:

$0 < n < 1$ and $k_1 > 0$.
From the Eqn. (4)

When $\dot{\gamma} \to \infty \Rightarrow \tau_{max.} = \infty$

Hence Herschel-Bulkley model doesn't satisfy the upper limit condition for the shear stress limit.

Vipulanandan model (2014)

Hyperbolic relationship between shear stress and shear strain rate for the spacer fluids with different temperature was investigated (Vipulanandan and Mohammed 2014).

$$\tau - \tau_{o2} = \frac{\dot{\gamma}}{C + D*\dot{\gamma}}, \quad (7)$$

where τ: shear stress (Pa); τ_{o2}: yield stress (Pa); C (Pa. s)$^{-1}$ and D (Pa)$^{-1}$: are model parameters and $\dot{\gamma}$: shear strain rate (s^{-1}). By applying the conditions from Eqns. (5), (6) and (7), following conditions are obtained for the parameters:

$$\frac{d\tau}{d\dot{\gamma}} = \frac{(C + D\dot{\gamma}) - \dot{\gamma} * D}{(C + D\dot{\gamma})^2} = \frac{C}{(C + D\dot{\gamma})^2} > 0 \Rightarrow C > 0$$

$$\frac{d^2\tau}{d\dot{\gamma}^2} = \frac{-2CD}{(C + D\dot{\gamma})^3} < 0 \Rightarrow D > 0.$$

Also when $\dot{\gamma} \to \infty \Rightarrow \tau_{\max} = \frac{1}{D} + \tau_{o2}$. (8)

Hence this model has a limit on the maximum shear stress; the slurry will produce at relatively high rate of shear strains.

Results and Analysis

Density

The density of the spacer fluid was 8.46 ppg. With the addition of 0.5% and 1% nanoFe_2O_3 (based on total weight of the spacer fluid) increased the density to 8.51 and 8.55 ppg. The density was increased by 0.6% with addition of 0.5% nanoFe_2O_3. The density also increased by 1% with the addition of 1% nanoFe_2O_3.

Electrical Resistivity

The spacer fluids with and without nanoFe_2O_3 were subjected to a temperature in the range of 25 to 75 C to investigate the change in electrical resistivity of the fluid.

T = 25°C: The resistivity of the smart spacer fluid increased with increase in the addition of nanoFe_2O_3 (Figure 1). The resistivity of the spacer fluid without and with 0.5% and 1% nanoFe_2O_3 were 0.2 Ω-m, 0.202 Ω-m and 0.207 Ω-m. At 25°C temperature, the increase in the electrical resistivity was 3.5%, with addition of 1% nanoFe_2O_3.

T = 50°C: The resistivity of the smart spacer fluid at 50 C increased linearly with addition of nanoFe_2O_3 content (Figure 1). The resistivity of the spacer fluid without, with 0.5% and 1% nanoFe_2O_3 were 0.182 Ω-m, 0.187 Ω-m and 0.193 Ω-m. At 50°C temperature, the increase in the electrical resistivity was 6%, with addition of 1% nanoFe_2O_3.

T = 75°C: The resistivity of the smart spacer fluid increased with increase in the addition of nanoFe_2O_3 (Figure 1). The resistivity of the spacer fluid without, with 0.5% and 1% nanoFe_2O_3 were 0.169 Ω-m, 0.172 Ω-m and 0.176 Ω-m. At 75°C temperature, the increase in the electrical resistivity was about 4%, with addition of 1% nanoFe_2O_3.
The electrical resistivity of the smart spacer fluid decreased from 0.2 Ω-m to 0.169 Ω-m, a 15 % decrease with the increase in temperature from 25 to 75°C.

Piezoresistivity

The smart spacer fluids with and without nanoFe_2O_3 were subjected to pressure up to 500 psi in the high pressure high temperature chamber (HPHT) to investigate the piezoresistive behavior.

NanoFe_2O_3 = 0%: The resistivity of the spacer fluid decreased nonlinearly with increase in the pressure (Figure 2). At 500 psi pressure the decrease in the resistivity was 0.7%, indicating low piezoresistivity characteristics of the spacer fluid.

NanoFe_2O_3 = 1%: The resistivity of the smart cement slurry with 1% nanoFe_2O_3 decreased nonlinearly with increase in the pressure (Figure 2). At 500 psi pressure the decrease in resistivity was 8%, indicating the piezoresistivity characteristics of the smart spacer fluid.

Rheology

Effect of NanoFe_2O_3

Shear stress – shear strain rate relationships were predicted using the Vipulanandan rheological model and compared with the Bingham Plastic and Hershel Bulkley models, as shown in Figure 3.

Bingham model (1919)

The plastic viscosity (PV) and yield stress were determined using the Bingham plastic model. Increasing the nanoFe_2O_3 content in the spacer fluid increased the plastic viscosity and yield stress of the spacer fluid. The yield stress of the spacer fluid with 1% nanoFe_2O_3 increased from 12.34 Pa to 19.52 Pa at 25°C as shown in figure 3. The Plastic viscosity increased from 37 to 49 cP with addition of 1% nanoFe_2O_3 in the spacer fluid.

Herschel-Bulkley model (1926)

The root mean square of error (RMSE) for the Hershel Bulkley model varied between 1.34 to 2.3 Pa. The model parameter k for the spacer fluid at 25°C varied from 4.58 to 8.14 Pa.s^n as summarized in table 1. The model parameter n was in range of 0.29 to 0.33.

Vipulanandan Rheological model (2014)

The shear thinning behavior of the spacer fluid with and without nanoFe_2O_3 was modeled using the Vipulanandan rheological model up to a shear strain rate of 1024 s-1 (600 rpm). Increasing the nanoFe_2O_3 content in the spacer fluid increased the yield stress of the spacer fluid. The yield stress of the spacer fluid increased from 3.94 Pa to 6.63 Pa when nanoFe_2O_3 was increased from 0% to 1% at 25°C as shown in figure 3. The τ_{max} for the spacer fluid increased from 49.4 Pa to 65.5 Pa, 33% increase at the temperature of 25°C with 1% addition of nanoFe_2O_3 respectively as summarized in table 1. The root mean square of error was in range of 1.4 to 2.13 Pa.

Effect of Temperature

Bingham model (1919)

The spacer fluid with and without nanoFe_2O_3 showed decrease in rheological properties with the increase in temperature from 25 to 75°C. The Plastics viscosity of spacer fluid without nanoFe_2O_3 reduced from 37 to 30 cP, 19 % decrease and yield stress from 12.34 Pa to 10.06 Pa, 18.5% decrease as in figure 4. The Plastic Viscosity of the spacer fluid with 0.5% and 1% nanoFe_2O_3 were 41 and 41.7 cP. The yield stress for the spacer fluid with 0.5% and 1% nanoFe_2O_3 were 13.3 and 13 Pa.

Herschel-Bulkley model (1926)

The model parameter k for the spacer fluid with and without nanoFe_2O_3 at 75°C varied from 3.82 to 4.99 Pa.s^n as summarized in table 2. The model parameter n was in range of 0.32 to 0.34. The root mean square of error (RMSE) for the Hershel Bulkley model varied between 0.99 to 1.85 Pa.

Vipulanandan model (2014)

The shear thinning behavior of spacer fluids without and with nanoFe_2O_3 were tested and modeled using the Vipulanandan model up to a shear strain rate of 1024 s^{-1} (600 rpm). The average yield stress decreased from 3.31 to 2.94 with the addition of 1% nanoFe_2O_3 at 75°C. The Maximum shear stress (τmax) for the spacer fluid increased from 39 Pa to 52.9 Pa, 36% increase with the increase in nanoFe_2O_3 at temperature of 75°C. The root mean square of error was in range of 1.27 to 1.49 Pa. (Table 4)

Effect of Magnetic Field
Magnetic field = 0.3 T

Bingham model (1919)

The spacer fluid with nanoFe_2O_3 showed increase in rheological properties in the presence of magnetic field of 0.3 T (Figure 5). The Plastic viscosity increased from 37 to 53.6 cP, a 44% increase and yield stress from 12.3 Pa to 21.5 Pa, a 75% increase with addition of 1% nanoFe_2O_3 at 25°C.

Herschel-Bulkley model (1926)

The root mean square of error (RMSE) for the Hershel Bulkley model varied between 1.34 to 2.2 Pa. The model parameter k for the spacer fluid at 25°C varied from 4.58 to 8.97 Pa.s^n as summarized in table 3. The model parameter n was in range of 0.29 to 0.33 for spacer fluid with

different nanoFe_2O_3 contents at temperatures of 25°C under Magnetic Field Strength of 0.3 T (Table 3).

Vipulanandan model (2014)

Increasing the magnetic field strength from 0 T to 0.3 T, increased the yield stress from 3.94 to 7.7 Pa and τmax from 49.4 to 74.4 Pa for spacer fluid with different nanoFe_2O_3 contents at temperatures of 25°C. The maximum shear stress increased by 50% for increasing the magnetic field from 0 to 0.3 T as in figure 5. The root mean square of error was in range of 1.3 to 2.2 Pa (Table 3)

Magnetic field = 0.6 T

Bingham model (1919)

The spacer fluid with nanoFe_2O_3 showed increase in rheological properties in the presence of magnetic field of 0.6 T (Figure 6). The Plastic viscosity increased from 37 to 62 cP, a 67% increase and yield stress from 12.3 Pa to 24.3 Pa, a 97% increase with addition of 1% nanoFe_2O_3 at 25°C. (Figure 6 and Table 4).

Herschel-Bulkley model (1926)

The root mean square of error (RMSE) for the Hershel Bulkley model varied between 1.34 to 3 Pa. The model parameter k for the spacer fluid at 25°C varied from 4.58 to 9.96 Pa.s^n as summarized in table 4. The model parameter n was in range of 0.29 to 0.33 for Spacer Fluid with different nanoFe_2O_3 contents at temperatures of 25°C under Magnetic Field Strength of 0.6 T (Table 4).

Vipulanandan model (2014)

Increasing the magnetic field strength from 0 T to 0.6 T, increased the yield stress from 3.94 to 7.8 Pa and τmax from 49.4 to 84.7 Pa for spacer fluid with different nanoFe_2O_3 contents at temperatures of 25°C. The maximum shear stress increased by 71% for increasing the magnetic field from 0 to 0.6 T as in figure 6. The root mean square of error was in range of 1.3 to 2.2 Pa (Table 4).

Effect of Bentonite Contamination

Bentonite Contamination = 0.15%:

Bingham model (1919)

The spacer fluid with 0.15% bentonite showed increase in rheological properties with the increase in nanoFe_2O_3 content at temperature of 25 °C. The Plastics viscosity increased from 39.7 to 55.2 cP, 40 % increase and yield stress from 10.3 Pa to 18.2 Pa, 76% increase as in figure 7.

Herschel-Bulkley model (1926)

The root mean square of error (RMSE) for the Hershel Bulkley model varied between 1.08 to 3.38 Pa. The model parameter k for the spacer fluid at 25°C varied from 3.32 to 6.9 Pa.s^n as summarized in table 5. The model parameter n was in range of 0.32 to 0.37.

Vipulanandan model (2014)

The shear thinning behavior of spacer fluids with different nanoFe_2O_3 contents and contaminated with 0.15% bentonite were tested and modeled using the Vipulanandan model up to a shear strain rate of 1024 s^{-1} (600 rpm). The average yield stress for the spacer fluid without nanoFe_2O_3 was 2.91 Pa which increased with the increase in the addition of nanoFe_2O_3, showing 14 % increase. The τmax for the spacer fluid increased from 50.5 Pa to 70 Pa, 38.6% increase with the increase in the addition of nanoFe_2O_3 at temperature of 25 °C. The root mean square of error was in range of 1.41 to 1.56 Pa. (Table 5)

Bentonite Contamination = 0.3%:

Bingham model (1919)

The spacer fluid with 0.3% bentonite contamination showed increase in rheological properties with the increase in nanoFe_2O_3 content at temperature of 25 °C. The Plastics viscosity increased from 39.4 to 57.1 cP, 45 % increase and yield stress from 11.25 Pa to 20.26 Pa, 80% increase as in Figure 8.

Herschel-Bulkley model (1926)

The root mean square of error (RMSE) for the Hershel Bulkley model varied between 1 to 3.98 Pa. The model parameter k for the spacer fluid at 25°C varied from 3.84 to 7 Pa.s^n as summarized in table 5. The model parameter n was in range of 0.31 to 0.36.

Vipulanandan model (2014)

The shear thinning behavior of spacer fluids with different nanoFe_2O_3 contents and contaminated with 0.3% bentonite were tested and modeled using the Vipulanandan model up to a shear strain rate of 1024 s^{-1} (600 rpm). The average yield stress for the spacer fluid without nanoFe_2O_3 was 3.81 Pa which decreased with the increase in the addition of nanoFe_2O_3, showing 15 % decrease. The τmax for the spacer fluid increased from 51.4 Pa to 74.7 Pa, 45.3% increase with the increase in the addition of nanoFe_2O_3 at temperature of 25 °C. The root mean square of error was in range of 1.4 to 1.9 Pa. (Table 6)

Bentonite Contamination = 0.5%:

Bingham model (1919)

The spacer fluid with 0.5% bentonite contamination showed increase in rheological properties with the increase in nanoFe_2O_3 content at temperature of 25 °C. The Plastics viscosity increased from 43.2 to 58.9 cP, 36 % increase and yield stress from 13 Pa to 22.7 Pa, 75% increase as in Figure 9.

Herschel-Bulkley model (1926)

The root mean square of error (RMSE) for the Hershel Bulkley model varied between 1.34 to 3.33 Pa. The model parameter k for the spacer fluid at 25°C varied from 4.57 to 9.36 Pa.s^n as summarized in table 5. The model parameter n was in range of 0.3 to 0.35.

Vipulanandan model (2014)

The shear thinning behavior of spacer fluids with different nanoFe_2O_3 contents and contaminated with 0.5% bentonite were tested and modeled using the Vipulanandan model up to a shear strain rate of 1024 s^{-1} (600 rpm). The average yield stress for the spacer fluid without nanoFe_2O_3 was 4.18 Pa which increased with the increase in the addition of nanoFe_2O_3, showing 41 % increase. The τmax for the spacer fluid increased from 56.8 Pa to 77.3 Pa, 36% increase with the increase in the addition of nanoFe_2O_3 at temperature of 25 °C. The root mean square of error was in range of 1.2 to 2.1 Pa (Table 7).

Cleaning Efficiency Test

The Bentonite Contamination used for cleaning efficiency test was 1% as calculated by $((W_2-W_1)*100/W_1)$ where W_1 is the weight of the empty sleeve in the viscometer and W_2 is the weight of the sleeve with bentonite mud. The cleaning efficiency test of the smart spacer fluid to effectively clean the bentonite drilling mud was performed as shown in figure 10(b). The cleaning efficiency of the spacer fluid was 82.3% without the addition of nanoFe_2O_3. With the addition of nanoFe_2O_3 the cleaning efficiency increased from 82.3 to 98.5%, 16.2% increase in the efficiency (Figure 10(a)).

The relation between maximum shear stress and cleaning efficiency for smart spacer fluid is as follows

$$\mathrm{CE}(\%) = \frac{\tau_{max}}{\mathrm{E} + \mathrm{F} * \tau_{max}} \quad (9)$$

Where CE = Cleaning efficiency in percentage,
τ_{max} = Maximum Shear Stress of the spacer fluid (Pa),
E, F = Model parameters.

The model parameters E and F are 0.49 Pa/percent and 0.0025 /percent respectively for the cleaning efficiency model. The R^2 and RMSE for the model are 0.99 and 1.53%. The maximum shear stress (τ_{max}) of the smart spacer fluid indicated the better cleaning ability of spacer fluid with 1% nanoFe_2O_3.(Figure 11(a)) The τ_{max} increased from 49.4 to 65.5 Pa, a 32.5% increase with the addition of 1% nanoFe_2O_3 while similarly the cleaning efficiency increased from 82 to 99% (Table 8). The main reason for the increased efficiency was having better rheological properties which produce higher shear stresses for cleaning and high surface to volume ratio of the nanoparticles. The maximum shear stress required to generate 100% cleaning efficiency was 65.5 Pa.

The relation between maximum shear stress and change in electrical resistivity for smart spacer fluid is as follows:

$$\mathrm{CE}(\%) = \mathrm{C}_o + \left(\frac{(\Delta\rho/\rho)}{\mathrm{G}+\mathrm{H}*(\Delta\rho/\rho)}\right) \quad (10)$$

Where CE = Cleaning efficiency in percentage,
C_o = Cleaning efficiency with no resistivity change (%),
$\Delta\rho/\rho$ = Change in Resistivity of the spacer fluid (%),
G, H = Model parameters.

The constant C_o for the spacer fluid cleaning efficiency vs resistivity change model is 49.8 %. The model parameters G and H were 0.084 and 0.0156 /percent. The R^2 and RMSE for the model are 0.99 and 1.358%. Change in electrical resistivity of smart spacer fluid measured before and after the test correlated with the cleaning efficiency of the smart spacer fluid. The Electrical resistivity increased after the test with the contamination spacer fluids with bentonite. The smart spacer fluid with 1% nanoFe_2O_3 showed maximum change in the resistivity, 16% due increased cleaning and higher amount of bentonite contamination in the spacer fluid (Figure 11(b)).

Effect of Bentonite Contamination

The relationship between Bentonite Contamination and resistivity of the smart spacer fluid is given by the following equation:

$$\mathrm{BC}(\%) = \frac{\rho - \rho_o}{\mathrm{M} + \mathrm{N}(\rho - \rho_o)} \quad (11)$$

Where BC = Bentonite Contamination in percentage,
ρ_o = Resistivity of the spacer fluid without oil (Ω-m), $(\rho \geq \rho_o)$
M, N = Model parameters.
The model parameters M and N are equal to 0.053 Ω-m/percent and 0.43 /percent for the smart spacer fluid. The R^2 and RMSE for the model are 0.99 and 0.01%. The electrical resistivity parameter was sensitive to changes in the spacer in real time. The electrical resistivity was found to increase with the increase in the Bulkley in the smart spacer fluid. The

resistivity of spacer fluid increased from 0.2 Ω-m to 0.35 Ω-m with addition of about 1.5 % Bulkley (Figure 12).
From the table 8, smart spacer fluid with 1% nanoFe_2O_3 showed a resistivity of 0.24 Ω-m after the cleaning efficiency test. The Bentonite Contamination in the spacer fluid is about 0.5% by weight of the smart spacer fluid (Figure 12). Electrical resistivity can be used as an indicator for the Bulkley and can also indicate the changes in the rheological properties in-situ.

Conclusions

In this study, effects of the magnetic field strengths, temperatures and bentonite contamination on the electrical resistivity and rheological properties of nanoFe_2O_3 modified spacer fluid were investigated. Also the rheological properties were correlated to the electrical resistivity. Based on the experimental study and analytical modeling following conclusions are advanced:

1. The electrical resistivity of the spacer fluid decreased with increasing temperature and it was a good sensing parameter for real-time monitoring to predict the rheological properties of spacer fluid in the field.

2. The addition of nanoFe_2O_3 up to 1% modified the yield stress, shear thinning behavior, and ultimate shear stress limit of the spacer fluid. The amounts of changes in the properties were influenced by the temperature, nanoFe_2O_3 content, and magnetic field strength in the spacer fluid and have been quantified using a nonlinear model.

3. The smart spacer fluid with nanoFe_2O_3 when contaminated with bentonite showed better rheological properties compared to spacer fluid without nanoFe_2O_3.

4. Electrical resistivity of the spacer fluid can be implemented in the field to identify the level of contamination, cleaning efficiency and change in rheological properties in real time.

Acknowledgements

This study was supported by the Center for Innovative Grouting Materials and Technology (CIGMAT) and Texas Hurricane Center for innovative Technology (THC-IT) at the University of Houston, Houston, Texas.

References

1. Afolabi, R., Oradu, O. D., Efeovbakhan, V.E. and Rotimi, O.J. (2017) Optimizing the Rheological Properties of Silica Nano-modified bentonite mud using overlaid contour plot and estimation of maximum or upper shear stress limit" Cognet Engineering, doi: 10.1080/23311916.2017.1287248.
2. Amanullah, M., and Al-Tahini, A. M. (2009). "Nano-technology-its significance in smart fluid development for oil and gas field application". *SPE Saudi Arabia Section Technical Symposium*. Society of Petroleum Engineers.
3. Harendra, S, and Vipulanandan, C. (2008). Degradation of High Concentrations of PCE Solubilized in SDS and Biosurfactant with Bimetallic Fe/Ni Particles, Colloids and Surfaces A: Physicochemical and Engineering Aspects, Vol. 322, No. 3, pp. 6-13.
4. Li L., Padilla, F., et al. (2016)."Evaluation of a New Spacer System Mixed On-The-Fly", AADE Fluids Technical Conference and Exhibition.
5. Livescu, S. (2012). "Mathematical modelling of thixotropic drilling mud and crude oil flow in wells and pipelines—a review". *Journal of Petroleum Science and Engineering*, *98*, 174-184.
6. Maserati, G., Daturi, E., et al. (2010)."Nano-emulsions as Cement Spacer Improve the Cleaning of Casing Bore during Cementing Operations", SPE Annual Technical Conference and Exhibition, 19-22 September, Florence, Italy.
7. Mohammed, A. (2017). Vipulanandan model for the rheological properties with ultimate shear stress of oil well PC modified with nanoclay, DOI 10.1016/j.ejpe.2017.05.007.
8. Olowolagba K, Yerubandi K.B. (2011). Improved spacer rheology model for cement operations. SPE 140805, SPE Production and Operations Symposium, Oklahoma, pp. 779-788.
9. Quintero, L., Christian, C., et al., (2008). "New Spacer Technology for Cleaning and Water Wetting of Casing and Riser", AADE Fluids Conference and Exhibition.
10. Remillard, S. C. (2010). "Applications of Nanotechnology within the Oil and Gas Industry," *Oil and Gas Review*, Vol. 8, pp. 1-108.
11. Sarap G.D. et al. (2009). "The use of high-performance spacers for zonal isolation in high-temperature high-pressure wells," SPE-124275-MS, Middle East Drilling Technology Conference & Exhibition, Manama, Bahrain, 26-28.
12. Theron BE, Bodin D, Fleming J. (2002). "Optimization of spacer rheology using neural network technology. SPE-74498-MS, IADC/SPE Drilling Conference, Dallas, Texas.
13. Tungittiplakorn, W., et al. (2005) "Engineered Polymeric Nano-particles for Bioremediation of Hydrophobic Contami- nants," *Environmental Science & Technology*, Vol. 39, No. 5, pp. 1354-1358.
14. Vipulanandan, C. and Ren, X. (2000) "Enhanced Solubilization and Biodegradation of Naphthalene with Biosurfactant," Journal of Environmental Engineering, ASCE, Vol. 126, No. 7, pp. 629-634.
15. Vipulanandan, C. and Mohammed, A., S. (2014) " Hyperbolic Rheological Model with Shear Stress Limit for Acrylamide Polymer Modified Bentonite Drilling Muds "Journal of Petroleum Science and Engineering, Vol. 122, pp.38-47.
16. Vipulanandan, C., and Amani, N. (2015a). "Behavior of nano Calcium Carbonate Modified Cement Contaminated with Oil Based Drilling Mud", Offshore Technology Conference, OTC-25845-MS.
17. Vipulanandan, C., and Mohammed, A., (2015b) "Effect of Nanoclay on the Electrical Resistivity and Rheological Properties of Smart and Sensing Bentonite Drilling Muds" Journal of Petroleum Science and Engineering, Vol. 130, pp. 86-95.

18. Vipulanandan, C., and Mohammed, A.(2017a). "Smart Bentonite Drillling Muds Modified with Iron Oxide Nanoparticles and Charaterized Based on the Electrical Resistivity and Rheological Properties with varying Magnetics field Strengths and Temperatures",Offshore Technology Conference, OTC-27626-MS.
19. Vipulanandan, C., and Mohammed, A. (2017b). "Rheological Properties of Piezoresistive Smart Cement Slurry Modified With Iron Oxide Nanoparticles for Oil Well Applications." Journal of Testing and Evaluation, ASTM, Vol. 45 Number 6, pp. 2050-2060.
20. Zanten, R.V., Deen, L. et al. (2011). "Successful Field Applications of Surfactant Nanotechnology to Displace Oil-based Drilling Fluids for Completion Operations", AADE National Technical Conference and Exhibition, Houston, Texas.

Table 1: Bingham Plastic, Herchel-Bulkley and Hyperbolic Rheological model parameters for smart spacer fluids with different nanoFe_2O_3 contents.

	Bingham Plastic Model		Hershel Bulkley Model				Vipulanandan Model				
Model Parameters	PV(cP)	Yield Stress (τ), Pa	n	k	τ (yield)	RMSE	C(Pa. s)$^{-1}$	D (Pa)$^{-1}$	τ (yield)(Pa)	τ (max)(Pa)	RMSE
NanoFe = 0%	37	12.34	0.33	4.58	0	1.34	3.43	0.022	3.94	49.4	1.39
NanoFe = 0.5%	44	17.93	0.29	7.61	0	2.3	1.95	0.019	5.43	58.1	1.7
NanoFe = 1%	49	19.52	0.29	8.14	0	2.03	1.99	0.017	6.63	65.5	2.13

Table 2:Bingham Plastic, Herchel-Bulkley and Hyperbolic Rheological model parameters for Spacer Fluid with different nanoFe_2O_3 contents at temperature of 75°C.

	Bingham Plastic Model		Hershel Bulkley Model				Vipulanandan Model				
Model Parameters	PV(cP)	Yield Stress (τ), Pa	n	k	τ (yield)	RMSE	C(Pa. s)$^{-1}$	D (Pa)$^{-1}$	τ (yield)(Pa)	τ (max)(Pa)	RMSE
NanoFe = 0%	29.8	10.06	0.33	3.82	0	0.99	4.17	0.028	3.31	39.0	1.27
NanoFe = 0.5%	41	13.3	0.33	4.99	0	1.99	2.56	0.021	2.98	50.6	1.42
NanoFe = 1%	41.7	13.04	0.34	4.77	0	1.85	2.67	0.02	2.94	52.9	1.49

Table 3:Bingham Plastic, Herchel-Bulkley and Hyperbolic Rheological model parameters for Spacer Fluid with different nanoFe_2O_3 contents at temperature of 25°C under Magnetic Field Strength of 0.3 T.

	Bingham Plastic Model		Hershel Bulkley Model				Vipulanandan Model				
Model Parameters	PV(cP)	Yield Stress (τ), Pa	n	k	τ (yield)	RMSE	C(Pa. s)$^{-1}$	D (Pa)$^{-1}$	τ (yield)(Pa)	τ (max)(Pa)	RMSE
NanoFe = 0%	37	12.34	0.33	4.6	0	1.34	3.44	0.022	3.94	49.4	1.39
NanoFe = 0.5%	42	16.1	0.3	7.6	0	1.81	2.09	0.018	6.35	61.9	2.07
NanoFe = 1%	53.6	21.5	0.29	9	0	2.2	1.91	0.015	7.70	74.4	2.2

Table 4: Bingham Plastic, Herchel-Bulkley and Hyperbolic Rheological model parameters for Spacer Fluid with different nanoFe_2O_3 contents at temperature of 25°C under Magnetic Field Strength of 0.6 T.

	Bingham Plastic Model		Hershel Bulkley Model				Vipulanandan Model				
Model Parameters	PV(cP)	Yield Stress (τ), Pa	n	k	τ (yield)	RMSE	C(Pa. s)$^{-1}$	D (Pa)$^{-1}$	τ (yield)(Pa)	τ (max)(Pa)	RMSE
NanoFe = 0%	37	12.34	0.33	4.6	0	1.34	3.44	0.022	3.94	49.4	1.39
NanoFe = 0.5%	53.2	21.7	0.29	9.2	0	3.01	1.49	0.016	5.95	68.5	1.74
NanoFe = 1%	62	24.3	0.3	10	0	3	1.58	0.013	7.80	84.7	2.01

Table 5: Bingham Plastic, Herchel-Bulkley and Hyperbolic Rheological model parameters for Spacer Fluid with different nanoFe_2O_3 contents and 0.15% bentonite contamination at temperature of 25°C.

	Bingham Plastic Model		Hershel Bulkley Model				Vipulanandan Model				
Model Parameters	PV(cP)	Yield Stress (τ), Pa	n	k	τ (yield)	RMSE	C(Pa. s)$^{-1}$	D (Pa)$^{-1}$	τ (yield)(Pa)	τ (max)(Pa)	RMSE
NanoFe = 0%	39.7	10.31	0.38	3.32	0	1.08	4.2	0.021	2.91	50.5	1.41
NanoFe = 0.5%	46.3	15.01	0.34	5.62	0	2.6	2.1	0.019	2.81	55.4	1.35
NanoFe = 1%	55.2	18.24	0.33	6.9	0	3.38	1.71	0.015	3.31	70.0	1.56

Table 6: Bingham Plastic, Herchel-Bulkley and Hyperbolic Rheological model parameters for Spacer Fluid with different nanoFe_2O_3 contents and 0.3% bentonite contamination at temperature of 25°C.

	Bingham Plastic Model		Hershel Bulkley Model				Vipulanandan Model				
Model Parameters	PV(cP)	Yield Stress (τ), Pa	n	k	τ (yield)	RMSE	C(Pa. s)$^{-1}$	D (Pa)$^{-1}$	τ (yield)(Pa)	τ (max)(Pa)	RMSE
NanoFe = 0%	39.4	11.25	0.36	3.84	0	1	4.08	0.021	3.81	51.4	1.88
NanoFe = 0.5%	50.7	16.18	0.34	6	0	3.02	1.92	0.016	2.73	65.2	1.25
NanoFe = 1%	57.14	20.26	0.32	7.99	0	3.98	1.39	0.014	3.24	74.7	1.58

Table 7: Bingham Plastic, Herchel-Bulkley and Hyperbolic Rheological model parameters for Spacer Fluid with different nanoFe_2O_3 contents and 0.5% bentonite contamination at temperature of 25°C.

	Bingham Plastic Model		Hershel Bulkley Model				Vipulanandan Model				
Model Parameters	PV(cP)	Yield Stress (τ), Pa	n	k	τ (yield)	RMSE	C(Pa. s)$^{-1}$	D (Pa)$^{-1}$	τ (yield)(Pa)	τ (max)(Pa)	RMSE
NanoFe = 0%	43.2	13.02	0.35	4.57	0	1.34	3.41	0.019	4.18	56.8	1.52
NanoFe = 0.5%	53.3	17.26	0.33	6.42	0	2.83	1.96	0.015	3.61	70.3	1.23
NanoFe = 1%	58.9	22.74	0.3	9.36	0	3.33	1.44	0.014	5.89	77.3	2.16

Table 8: Cleanng efficiency, Maximum Shear Stress and Resistivity changes during cleaning efficeicny test for Spacer Fluid with different nanoFe_2O_3 contents.

Spacer	Cleaning Efficiency (%)	τ_{max} (Pa)	Resistivity (Ω-m)		Resistivity Change (%)
			Before Test	After Test	
NanoFe = 0%	82.3	49.4	0.2	0.209	4
NanoFe = 0.5%	92.2	58.1	0.202	0.226	12
NanoFe = 1%	98.5	65.5	0.207	0.24	16

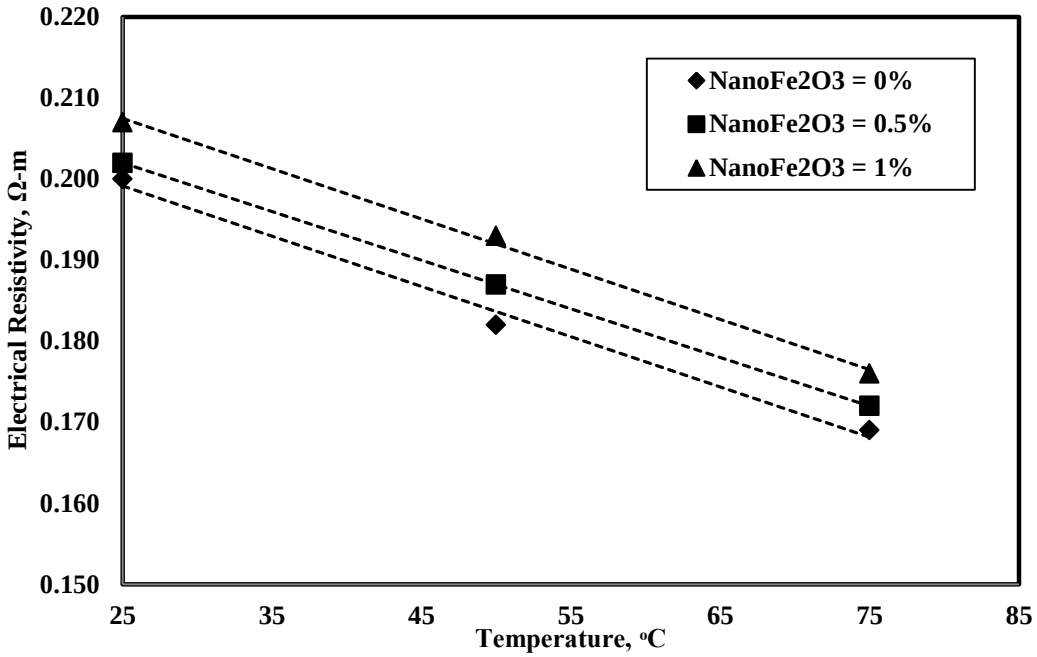

Figure 1. Effect of temperature on the electrical resistivity of spacer fluid with different nanoFe_2O_3 contents.

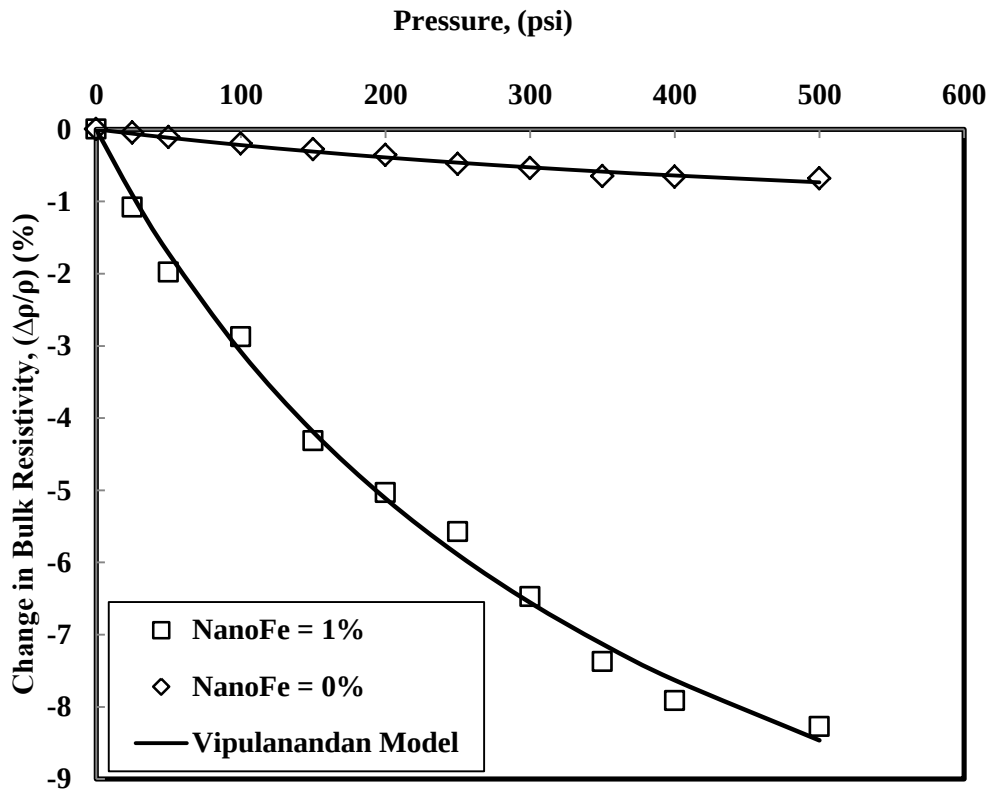

Figure 2. Measured and predicted stress-resistivity relationship for the smart spacer fluid with different nanoFe_2O_3 contents.

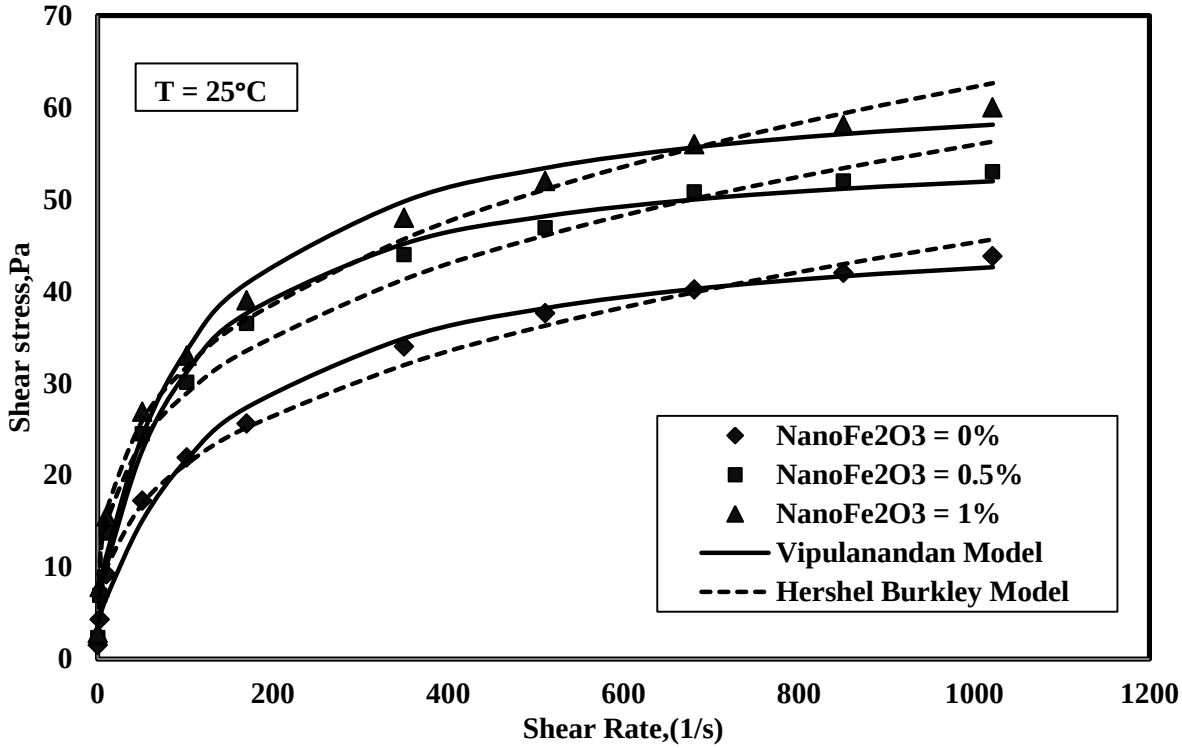

Figure 3. Shear Stress- Shear Strain rate Relationship for Spacer Fluid different nanoFe_2O_3 contents at 25°C.

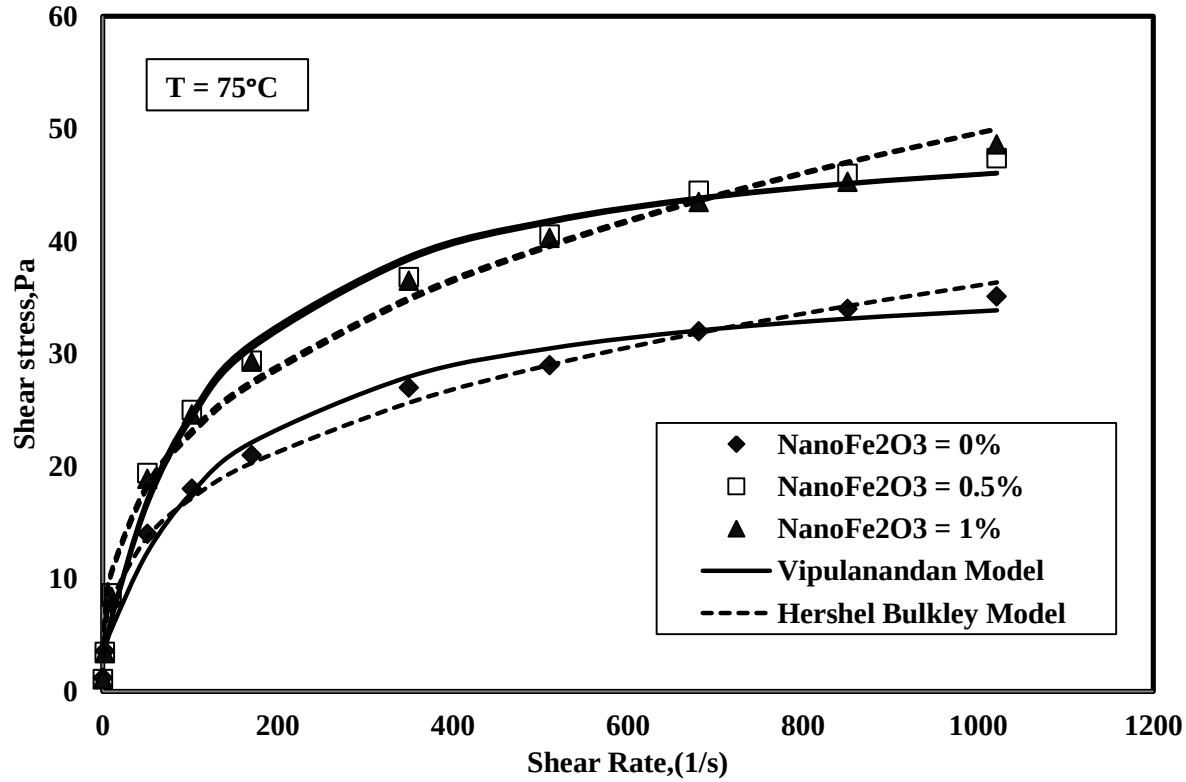

Figure 4. Shear Stress- Shear Strain rate Relationship for Spacer Fluid with different nanoFe_2O_3 contents at temperature of 75°C.

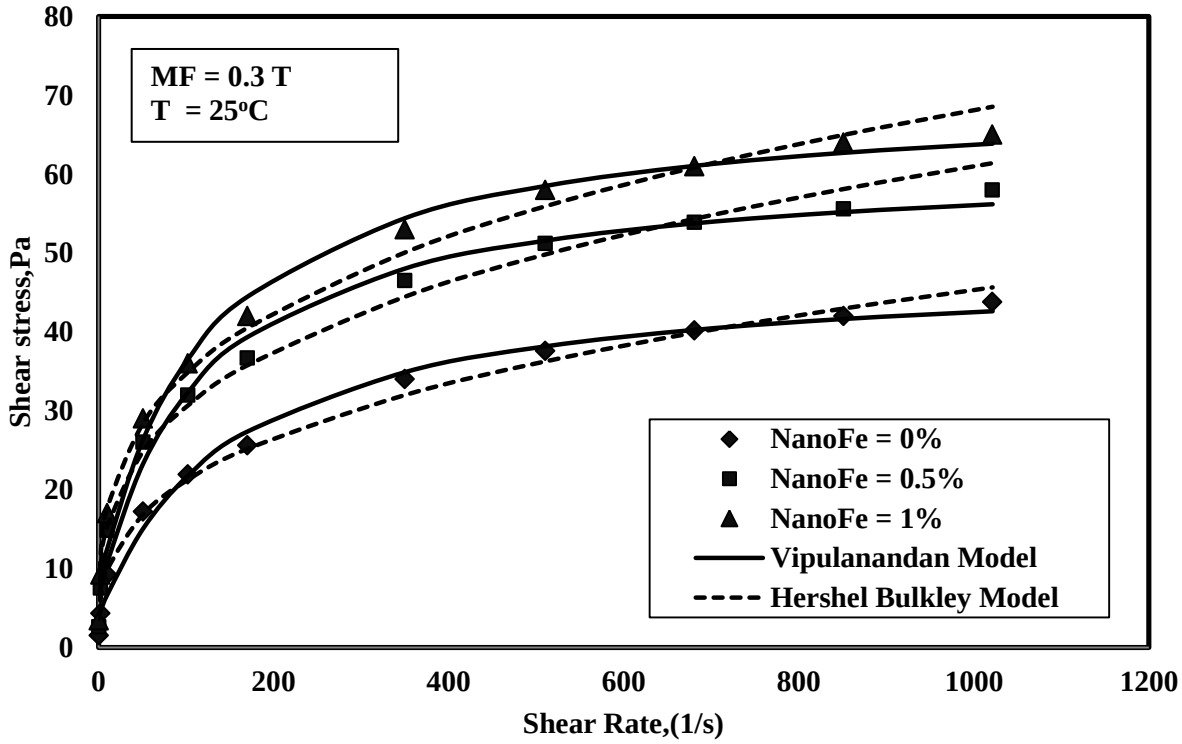

Figure 5. Shear Stress- Shear Strain rate Relationship for Spacer Fluid with different nanoFe2O3 contents at temperature of 25°C under Magnetic Field Strength of 0.3 T.

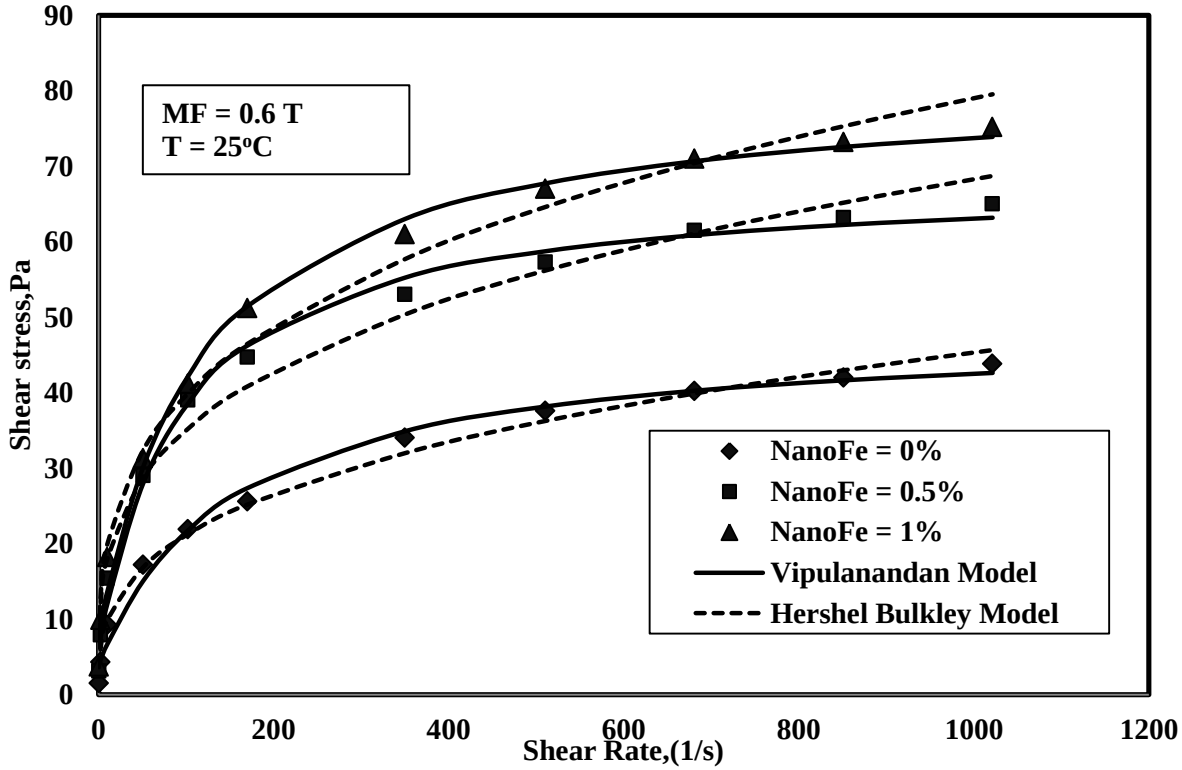

Figure 6. Shear Stress- Shear Strain rate Relationship for Spacer Fluid with different nanoFe2O3 contents at temperature of 25°C under Magnetic Field Strength of 0.6 T.

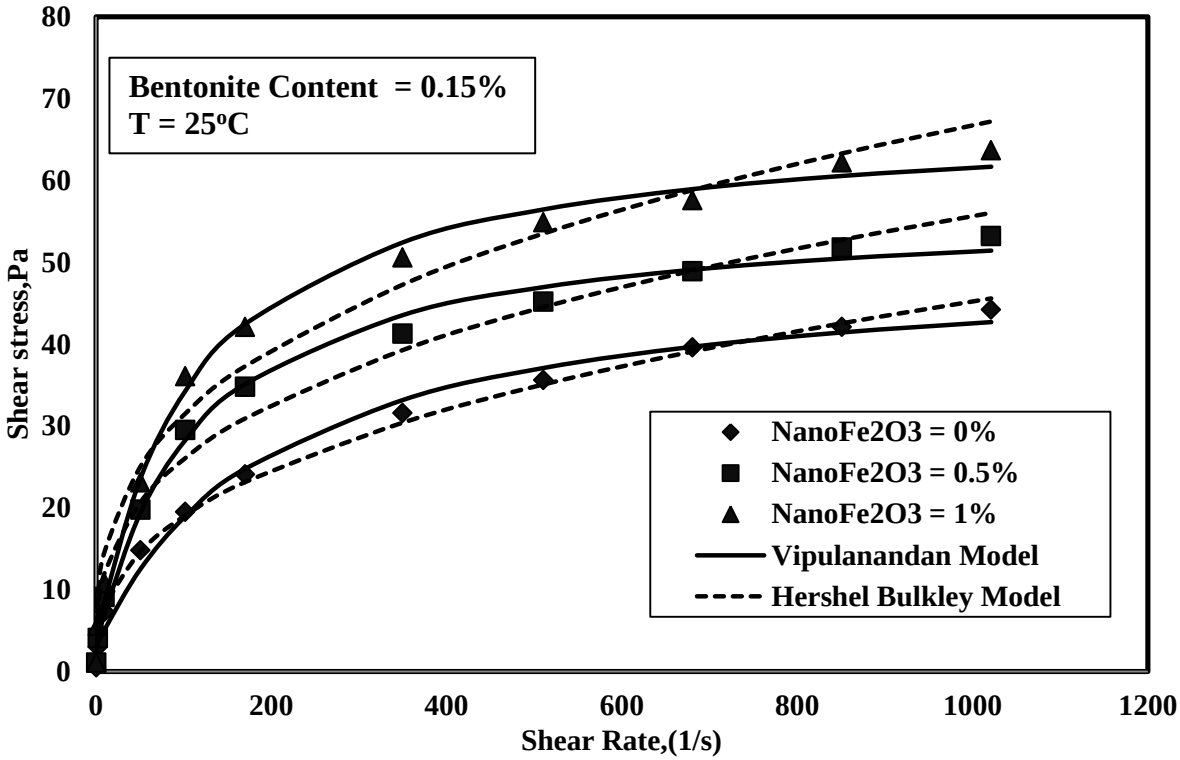

Figure 7. Shear Stress- Shear Strain rate Relationship for Spacer Fluid with different nanoFe2O3 contents and 0.15% bentonite contamination at temperature of 25°C.

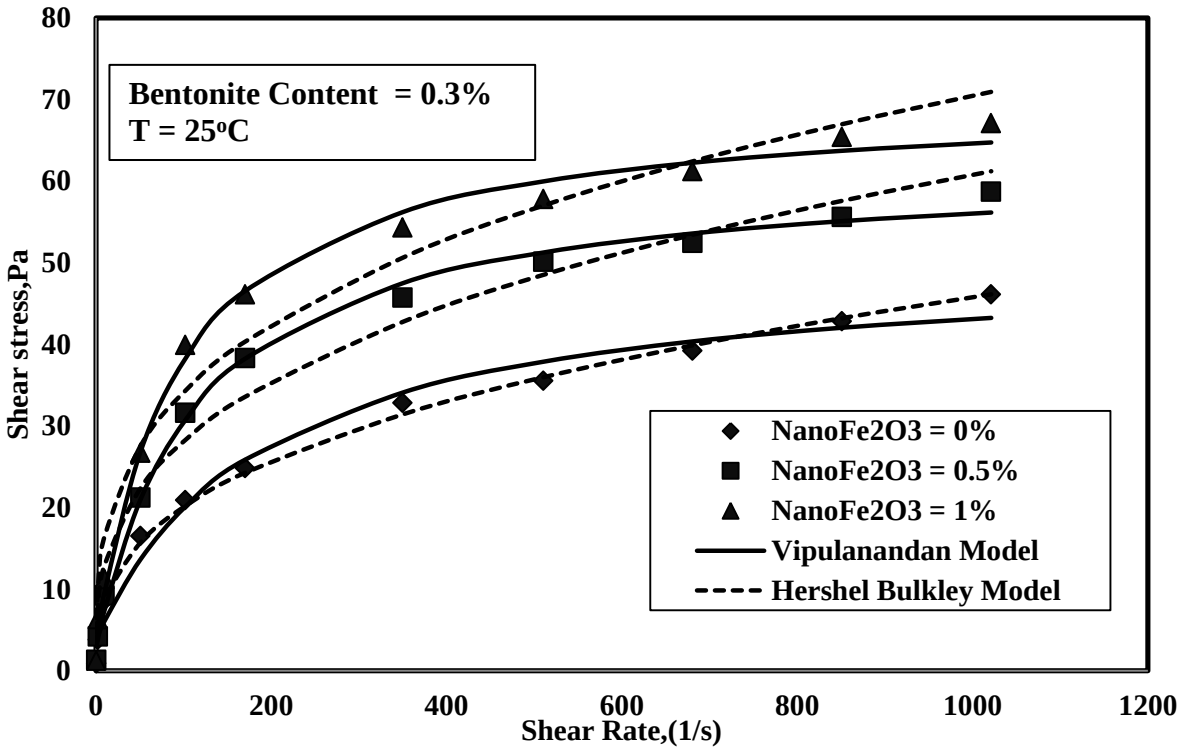

Figure 8. Shear Stress- Shear Strain rate Relationship for Spacer Fluid with different nanoFe2O3 contents and 0.3% bentonite contamination at temperature of 25°C.

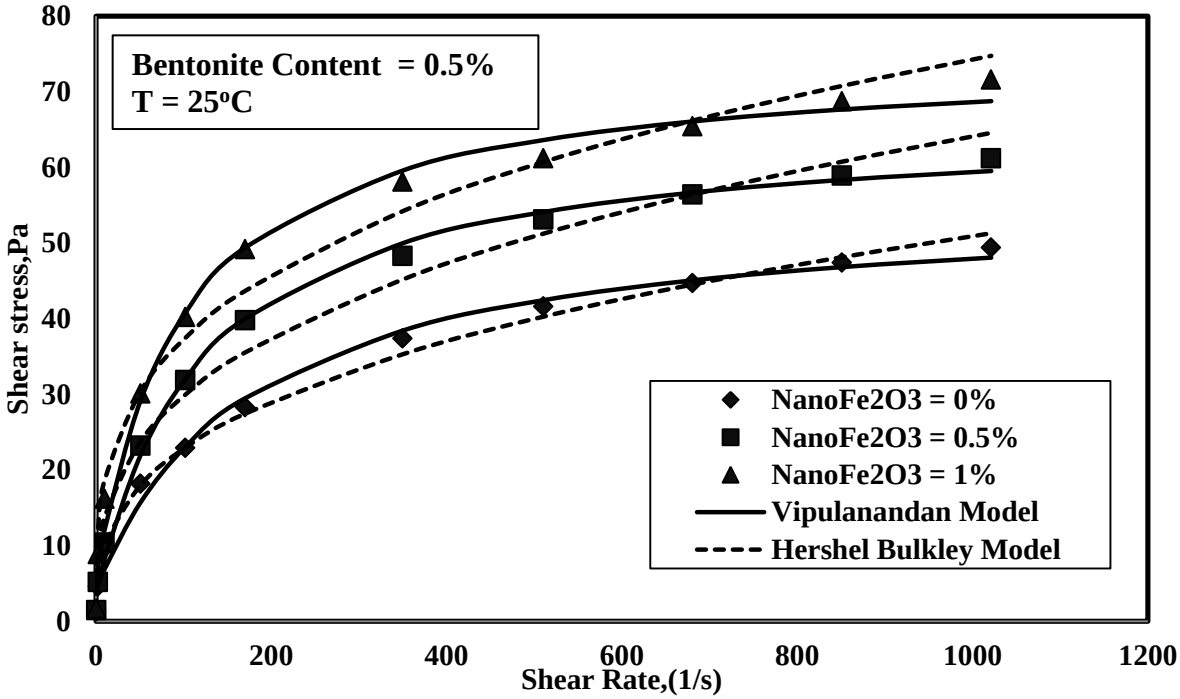

Figure 9. Shear stress- shear strain rate Relationship for Spacer Fluid with different nanoFe2O3 contents and 0.5% bentonite contamination at temperature of 25°C.

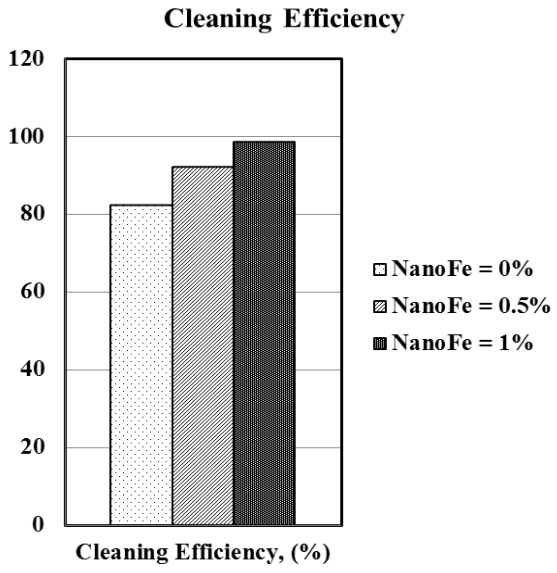

Figure 10(a). Cleaning efficiency of spacer fluid different nanoFe2O3 contents.

Figure 10(b). Cleaning efficiency test of bentonite drilling muds using Viscometer.

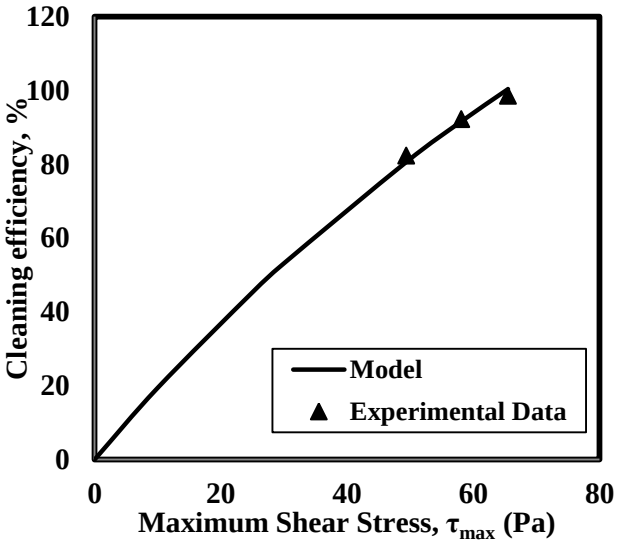

Figure 11(a). Relation between maximum shear stress (τ_{max}) and cleaning efficiency of the spacer fluid.

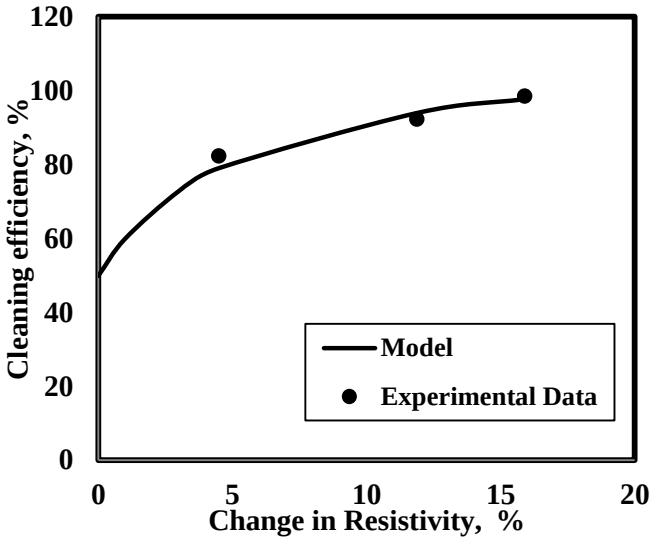

Figure 11(b). Relation between change in resistivity and cleaning efficiency of the spacer fluid.

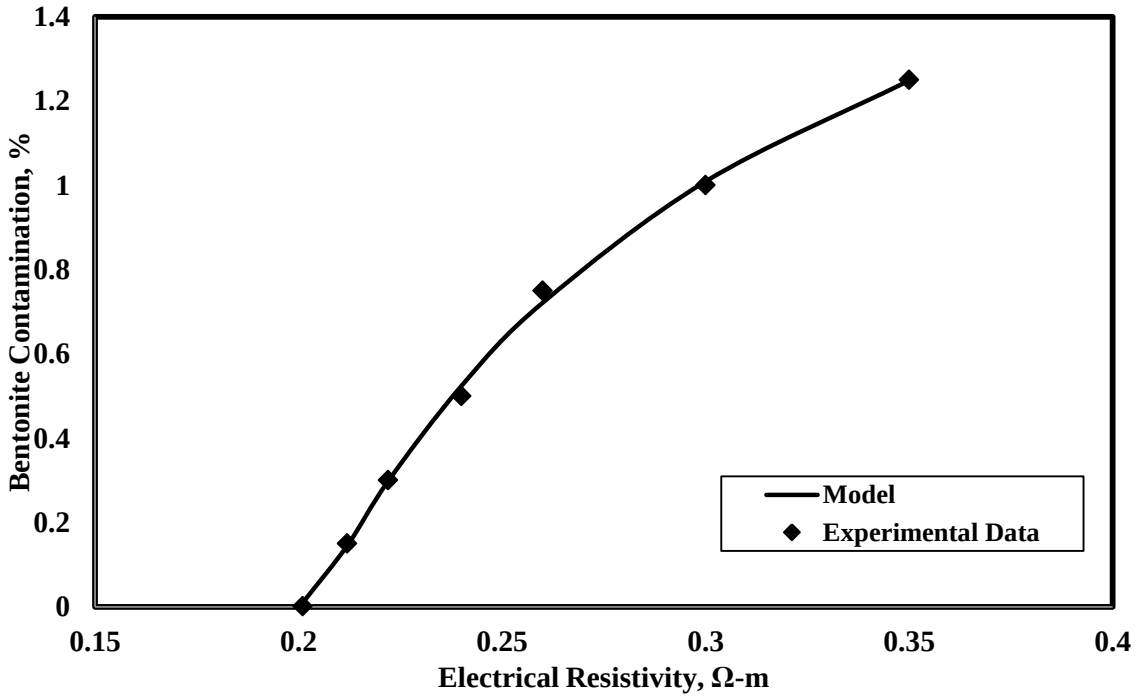

Figure 12. Variation of resistivity of the spacer fluid with bentonite contamination.